

# DARKFARSEER: Inductive Spatio-temporal Kriging via Hidden Style Enhancement and Sparsity-Noise Mitigation

Zhuoxuan Liang, Wei Li, *Member, IEEE*, Dalin Zhang, *Senior Member, IEEE*, Yidan Chen, Zhihong Wang, Xiangping Zheng and Moustafa Youssef, *Fellow, IEEE*

**Abstract**—With the rapid growth of the Internet of Things (IoT) and Cyber-Physical Systems (CPS), widespread sensor deployment has become essential. However, the high costs of building sensor networks limit their scale and coverage, making fine-grained deployment challenging. Inductive Spatio-Temporal Kriging (ISK) addresses this issue by introducing virtual sensors. Based on graph neural networks (GNNs) extracting the relationships between physical and virtual sensors, ISK can infer the measurements of virtual sensors from physical sensors. However, current ISK methods rely on conventional message-passing mechanisms and network architectures, without effectively extracting spatio-temporal features of physical sensors and focusing on representing virtual sensors. Additionally, existing graph construction methods face issues of sparse and noisy connections, destroying ISK performance. To address these issues, we propose DARKFARSEER, a novel ISK framework with three key components. First, we propose the Neighbor Hidden Style Enhancement module with a style transfer strategy to enhance the representation of virtual nodes in a temporal-then-spatial manner to better extract the spatial relationships between physical and virtual nodes. Second, we propose Virtual-Component Contrastive Learning, which aims to enrich the node representation by establishing the association between the patterns of virtual nodes and the regional patterns within graph components. Lastly, we design a Similarity-Based Graph Denoising Strategy, which reduces the connectivity strength of noisy connections around virtual nodes and their neighbors based on their temporal information and regional spatial patterns. We examine existing graph construction approaches with preliminary experiments, identify their limitations, and motivate our work. Extensive experiments demonstrate that DARKFARSEER significantly outperforms existing ISK methods, e.g., the improvement in MAE score reaching as high as 10.58%.

**Index Terms**—Spatial-temporal kriging, graph modeling, contrastive learning

## I. INTRODUCTION

THE rapid advancement and widespread adoption of the Internet of Things (IoT) and Cyber-Physical Systems (CPS) have substantially increased the demand for fine-grained and ubiquitous sensing. Consequently, deploying huge amounts of sensors has become a common aspiration among

practitioners in various fields [1]–[3]. However, the high costs of sensor deployment pose significant challenges to this request. To address this limitation, *Spatio-temporal Kriging* (SK) has emerged, which introduces the concept of virtual sensors and aims to estimate the readings of virtual sensors based on those of physically deployed sensors. SK is generally divided into two branches: *Transductive SK* (TSK) and *Inductive SK* (ISK). TSK assumes prior access to the spatial information of virtual sensors before inference, while ISK only acquires this information during inference, making it a more practical and appealing solution in real-world applications. Following previous SK studies [4]–[7], this paper focuses on the ISK task to further explore its potential.

Deep learning-based methods [4], [5], [7]–[10], representing the state-of-the-art (SOTA) in ISK, predominantly rely on Graph Neural Networks (GNNs) to model the relationships between physical and virtual sensors (i.e., nodes in a graph). However, existing approaches primarily employ generic GNN architectures without accounting for the unique characteristics of the ISK task, leading to limitations in both graph construction and network design.

- **L1: Lack of specific message-passing design in GNNs for virtual nodes.** Generic GNN architectures [4], [5], [7], [9] treat all nodes equally, as their primary objective is to capture the overall spatial information of the graph. The message-passing process progressively aggregates information from  $N$ -hop neighbors to represent virtual nodes and derive an embedding for the entire graph. However, the ISK task has a distinct focus: inferring the values of virtual nodes. This task benefits more from prioritizing information from the immediate neighboring nodes of virtual sensors rather than aggregating data from the entire graph. Moreover, simple weighted aggregation is insufficient to capture the complex relationships between virtual nodes and their neighbors. Specific message-passing design is therefore desired for the ISK context.
- **L2: Limitations of spatial-first network structures in modeling spatial relationships.** Existing GNNs for ISK primarily adopt a spatial-first approach, where spatial information is processed before temporal information is embedded. However, this spatial processing relies on node embeddings derived directly from raw time series data, prior to temporal embedding. As a result, the spatial-then-temporal approach fails to fully leverage the potential of

Corresponding author: Wei Li.

Zhuoxuan Liang, Wei Li, Yidan Chen, Zhihong Wang and Xiangping Zheng are with the College of Computer Science and Technology, Harbin Engineering University, Harbin, 150001, China. E-mail: {zz.liang, wei.li, chen.yidan, 1084472397, xpzhang}@hrbeu.edu.cn.

Dalin Zhang is with the Spatial Information Research Institute, Hangzhou Dianzi University, Hangzhou, 310018, China. E-mail: zhangdalin@hdu.edu.cn

Moustafa Youssef is with the American University in Cairo, Egypt. E-mail: moustafa-youssef@aucegypt.edu

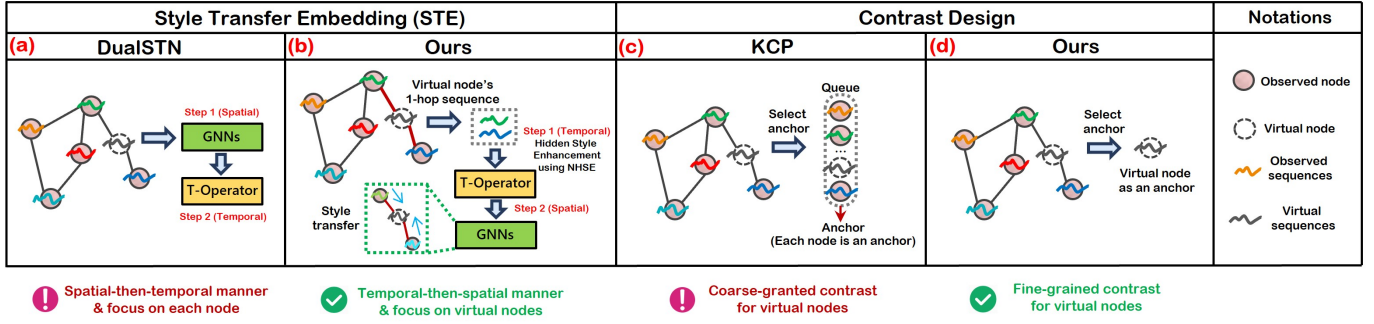


Fig. 1. Comparison of existing work and our DARKFARSEER: Unlike DualSTN in Fig 1(a), our STE Module is structured temporal-then-spatial, enhancing the hidden style of virtual node neighbors and performing style transfer (Fig 1(b)). Fig 1(d) highlights the unique aspect of our contrast design, using only virtual nodes as anchors, unlike KCP in Fig 1(c).

spatial message passing, which is crucial for the ISK task.

- **L3: Sparsity in graph structures.** We conducted comprehensive statistical analyses and preliminary experiments using a typical GNN-based ISK method [4] across various datasets (see Section §III.B). The results reveal that some datasets, particularly where node distances are determined through expert intervention (referred to as PCGs), exhibit graph structures with extreme edge sparsity (see Section §III.B.1). This sparsity leads to insufficient information from neighboring nodes, hindering the inference of virtual node values and ultimately compromising the performance of the ISK task.
- **L4: Noise in graph structures.** In contrast to sparse graph structures, some datasets exhibit extreme edge density, particularly in graphs constructed based on geographical proximity (referred to as SPGs). While such high density ensures sufficient neighboring information, it also inevitably introduces noise, as less relevant neighbors contribute to the embeddings of virtual nodes. Both sparsity and noise adversely impact kriging performance (see Section §III.B), which should be carefully handled.

Considering these limitations, we first conduct a comprehensive investigation to experimentally showcase the sparsity and noise issues in current graph structures. Then, we propose DARKFARSEER, which addresses these limitations and thus achieves new SOTA performance in ISK tasks.

To address L1 and L2, we propose Neighbor Hidden Style Enhancement (NHSE). As shown in Fig 1(a), existing methods such as DualSTN [9], follow a spatial-then-temporal manner, whereas our NHSE module proposes to first embed temporal features using T-operator (e.g., GRUs) and then process spatial information, that is the temporal-then-spatial manner, as shown in 1(b). In the spatial feature extraction, we propose to construct the graph structure with only 1-hop neighbors of virtual nodes to focus on representing the virtual nodes. Furthermore, we propose a style transfer [11], [12] strategy to transfer the temporal fluctuation patterns of the 1-hop physical node neighbors to virtual nodes, to enhance their representations. The temporal style transfer strategy can be seamlessly integrated with various kriging backbones (e.g., GNNs), significantly improving ISK performance (see §V.F).

To address L3, we propose Virtual-Component Contrastive

Learning (VCCL), which utilizes regional information as contrastive samples rather than relying solely on individual nodes. This approach enriches the representation of nodes with sparse spatial relationships, effectively addressing the sparsity issue. Specifically, we first identify highly related subgraphs, i.e., Biconnected Components (BCCs), within the graph. These BCCs are then aggregated into prototypes [13], [14] to capture high-level regional information. Within the contrastive learning (CL) framework, we pull virtual nodes closer to their own prototypes while pushing them away from other prototypes, reinforcing the similarity between virtual nodes and their associated regions. Furthermore, unlike existing ISK CL methods [7], which use all nodes as anchors (coarse-grained contrast), VCCL exclusively employs virtual nodes as anchors for CL. This allows our model to focus on modeling the patterns of virtual nodes (fine-grained contrast), as illustrated in Fig 1(c) and Fig 1(d). Through this approach, VCCL enhances the embedding of virtual nodes, particularly those with sparse spatial connections.

To address L4, we propose the Similarity-based Graph Denoising Strategy (SGDS). SGDS performs denoising on the relationships between virtual nodes and their neighbors to reduce the impact of graph noise. Specifically, SGDS evaluates both the temporal similarity between each virtual node and its neighbors, as well as the similarity to prototypes, in order to selectively reduce the connection density of noisy edges.

The contributions of this paper are summarized as:

- We conduct a thorough investigation and analysis of existing graph construction methods, and through preliminary experiments, demonstrate that the two current types of graphs are limited by sparsity and noise in ISK tasks (Section §III).
- We introduce NHSE, which proposes the temporal-then-spatial manner and the temporal style transfer strategy to effectively focus on virtual nodes to enhance virtual node representations (Section §IV.B).
- We propose VCCL and SGDS to mitigate the sparsity and noises of graphs to enhance the learning process of virtual node representation via contrastive learning (Section §IV.C and §IV.D).
- We study DARKFARSEER on various datasets while considering seven baselines, providing evidence of SOTA performance. We also provide a comprehensive analysis of various

aspects of DARKFARSEER (Section §V).

Besides, Section §II provides the formal problem definitions, Section §III presents the analysis and motivation related to graph structures, Section §VI covers related work on kriging and graph modeling for time series, and Section §VII concludes the whole paper.

## II. PROBLEM DEFINITION

### A. Spatio-temporal Kriging (SK)

Given the readings  $\mathbf{X}_{t:t+T}^o \in \mathbb{R}^{N_o \times T}$  of  $N_o$  physical sensors  $L^o = \{l_i\}_1^{N_o}$ , the goal of SK is to infer the readings  $\mathbf{X}_{t:t+T}^u \in \mathbb{R}^{N_u \times T}$  of  $N_u$  virtual sensors  $L^u = \{l_i\}_1^{N_u}$ , based on their spatial relationships (e.g., distance).  $\mathbf{X}_{t:t+T}^o$  and  $\mathbf{X}_{t:t+T}^u$  are essentially multivariate time series. The spatial relationships can be formulated as a collection of triplets  $R = \{(l_i, l_j, d_{l_i, l_j}) \mid l_i \in L^o, l_j \in L^u\}$ , where  $d_{l_i, l_j}$  is the distance between  $l_i$  and  $l_j$ .

1) *Transductive SK (TSK)*: In TSK, virtual sensors and the complete spatial relationships  $R$  are accessible during training. Let  $\mathcal{F}$  denote a kriging model. The kriging during training and inference for TSK can be formulated as:

$$\hat{\mathbf{X}}_{t:t+p}^u = \mathcal{F}(\mathbf{X}_{t:t+p}^o, R), \quad (1)$$

where  $p$  represents the time window size.

2) *Inductive SK (ISK)*: In contrast, ISK only accesses the virtual sensors and the complete spatial relationships  $R$  during the inference phase. The kriging during training can be formulated as:

$$\hat{\mathbf{X}}_{t:t+p}^o = \mathcal{F}_{\text{train}}(\mathbf{X}_{t:t+p}^o, R^o), \quad (2)$$

where  $R^o = \{(l_i, l_j, D_{l_i, l_j}) \mid l_i, l_j \in L^o, i \neq j\}$  is the spatial relationships of the observed sensors. The inference phases for ISK can be formulated as:

$$\hat{\mathbf{X}}_{t:t+p}^u = \mathcal{F}_{\text{infer}}(\mathbf{X}_{t:t+p}^o, R). \quad (3)$$

During the training phase,  $\mathcal{F}_{\text{train}}$  is learned based on  $\mathbf{X}^o$  and their spatial relationships  $R^o$ . In the inference phase,  $\mathcal{F}_{\text{infer}}$  performs inference based on  $\mathbf{X}^o$  and the complete spatial relationships  $R$  between observed and virtual sensors. Since ISK is more challenging and practical, we focus on the ISK task in this paper.

### B. Graph-based ISK

By considering sensors as nodes  $\mathcal{V}$  and the reachability relationships between nodes as edges  $\mathcal{E}$ , sensors and their spatial relationships can be represented as a graph  $\mathcal{G} = (\mathcal{V}, \mathcal{E})$ . The spatial relationships  $R$  in ISK can be represented using an adjacency matrix  $\mathbf{A} \in \mathbb{R}^{N \times N}$ . On top of this, the training and inference phases of graph-based ISK can be expressed as:

$$\hat{\mathbf{X}}_{t:t+p}^o = \mathcal{F}_{\text{train}}(\mathbf{X}_{t:t+p}^o, \mathbf{A}^o), \text{ where } \mathbf{A}^o \in \mathbb{R}^{N_o \times N_o}, \quad (4)$$

$$\text{and } \hat{\mathbf{X}}_{t:t+p}^u = \mathcal{F}_{\text{infer}}(\mathbf{X}_{t:t+p}^o, \mathbf{A}), \text{ where } \mathbf{A} \in \mathbb{R}^{N \times N}. \quad (5)$$

## III. ANALYSIS AND MOTIVATION

In this section, we first investigate two types of graph structures (§III.A). Subsequently, we analyze the issues of inconsistent graph density (§III.B.1) and noisy edges (§III.B.2) present in the two graph construction methods. Finally, in §III.C, we motivate that providing topological prompts can alleviate graph sparsity, and designing edge-dropping strategies can mitigate graph density and reduce the limitations caused by noisy edges.

### A. Graphs for ISK

Deep learning-based kriging methods primarily rely on GNNs that necessitate constructing a graph to model the interrelationships of sensors (i.e., nodes in a graph). Heuristic-based Graphs [15] based on the distances between nodes is a common and effective approach [16]–[22]. There are generally two branches to constructing heuristic-based Graphs:

- *Pairwise Connectivity Graphs (PCGs)*: In this approach, the reachability and corresponding distance between two nodes are available according to expert intervention. Thus, the adjacency matrix can be built based on the pairwise distance:

$$\mathbf{A}_{i,j} = \begin{cases} d_{i,j} & \text{if node } i \text{ and } j \text{ are linked,} \\ 0 & \text{otherwise,} \end{cases} \quad (6)$$

where  $d_{i,j}$  is the distance between node  $i$  and  $j$ .

- *Spatial Proximity Graphs (SPGs)*: The reachability between nodes is unknown while the geographical coordinates of each node are available. Thus, it is essential to calculate the distance between any two nodes to construct a graph. The adjacency matrix can be formulated as:

$$\mathbf{A}_{i,j} = \begin{cases} \frac{\exp(-\|d_{i,j}\|_2)}{\sigma} & \text{if } \frac{\exp(-\|d_{i,j}\|_2)}{\sigma} < \varepsilon, \\ 0 & \text{otherwise.} \end{cases} \quad (7)$$

where  $d_{i,j}$  is the node distance,  $\sigma$  is a hyperparameter to normalize the distance distribution, and  $\varepsilon$  is the threshold to control the sparsity of the adjacency matrix.

Notably, PCGs rely on expert intervention to determine pairwise node distances, whereas SPGs achieve node connections based on geographic distances between nodes and the predefined threshold  $\varepsilon$ .

### B. Limitation Analysis

We conducted comprehensive preliminary experiments and made observations to confirm our conjectures and motivate the proposal of DARKFARSEER.

- 1) *Inconsistent Graph Density in PCGs*: In this section, we analyze the issues caused by inconsistent graph density (sparse or dense) in PCGs. Through preliminary experiments, we conclude that topological prompts can alleviate graph sparsity, and discarding some edges can mitigate graph density.

We investigate the generalization of three datasets, namely PEMS03, PEMS04 and PEMS-BAY, in two application scenarios: traffic flow and traffic speed. The statistical information is provided in TABLE I. The average degree indicates how many other nodes, on average, each node in the graph is connected

TABLE I  
STATISTICS FOR THE PAIRWISE CONNECTIVITY GRAPHS ACROSS THREE DATASETS.

Scenario	Traffic Flow		Traffic Speed
Dataset	PEMS03	PEMS04	PEMS-BAY
Nodes	358	307	325
Avg Degree	3.05	2.20	49.43
Std Degree	1.11	1.01	27.14

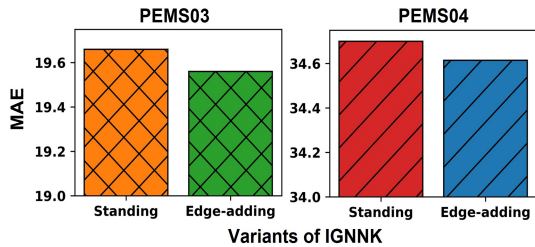


Fig. 2. MAE comparison of standing IGNNK and edge-adding IGNNK on traffic flow datasets.

to. It can be observed that the average degree of the graph formulated for traffic flow ranges from 2 to 4; **Conjecture I:** *fewer neighboring nodes may result in insufficient interaction between nodes. Effective topological information can alleviate this issue by enriching the node representations.* In contrast, for traffic speed, the average degree for PEMS-BAY is 49.43; **Conjecture II:** *not all neighbors of a node are relevant, and too many neighbors may introduce noise. Reducing some edges might alleviate this issue.* To investigate the aforementioned conjectures, we perform two groups of experiments using a classic graph-based ISK method named IGNNK [4].

- **Preliminary Experiment I:** To examine the conjecture I, we conduct edge-adding operations on the graphs of two traffic flow datasets. Specifically, during the training phase, we add edges between nodes and other nodes in their Biconnected Components (BCCs) to give IGNNK more topological prompts, considering that BCC, as a special subgraph, can represent local connectivity. The empirical findings are depicted in Fig 2. Following the application of edge-adding, the MAE of IGNNK witness a reduction. **Observation I:** The PCGs encounter constraints due to sparsity. Furthermore, these limitations can be mitigated by incorporating a topological prompt into the ISK model.
- **Preliminary Experiment II:** To verify the conjecture II, we perform edge-dropping operations on the graph constructed from PEMS-BAY. Specifically, we randomly remove edges from the graph with different probabilities during training. The empirical results are shown in Fig 3. We can see that when the drop edge rate is set to 0.1, IGNNK’s MAE decreases on PEMS-BAY. **Observation II:** The PCGs have a density limitation, i.e., too many edges will bring noise to the model. Therefore, designing noise reduction methods for the model can reduce this limitation.

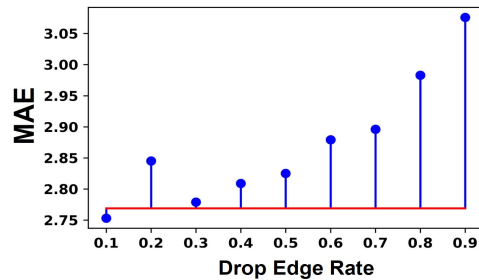


Fig. 3. MAE comparison of IGNNK with different edge-dropping rate on PEMS-BAY dataset. The red horizontal line represents the MAE of the standing IGNNK.

2) *Noise Edges in SPGs:* In this section, we analyze the issues caused by noise edges in SPGs. Through preliminary experiments, we observe that discarding some edges can mitigate the limitations introduced by noise edges. Note that,

TABLE II  
STATISTICS FOR THE SPATIAL PROXIMITY GRAPHS OVER TWO DATASETS.

Scenario	Air Quality		Solar Energy	
Dataset	AIR-36		NREL-PA	
Nodes	36		101	
Threshold $\epsilon$	0.1	0.9	0.1	0.9
Avg Degree	18.17	2.15	58.48	6.81
Std Degree	8.71	2.55	17.60	4.80

as mentioned in §III.A, compared to the edges in PCGs, which are influenced by expert intervention, there is less available information for constructing SPGs. Since calculating the geographical distance between each pair of nodes is a crucial step in constructing SPGs, and geographical distance often contains noise, given that geographical proximity does not invariably guarantee reachability between two nodes. TABLE II records the statistics of SPGs for the air quality and solar energy scenarios in two datasets, with threshold  $\epsilon$  set to 0.1 and 0.9. It can be observed that when  $\epsilon$  is 0.9, the average degree of the SPGs for AIR-36 and NREL-PA is between 2 and 7, which is relatively sparse. However, when  $\epsilon$  is 0.1, the average degree of the SPGs for these datasets is 18.17 and 58.48, respectively, which is relatively dense. **Conjecture III:** *Because the SPGs threshold  $\epsilon$  controls the graph density, we hypothesize that making the SPGs sparser can alleviate edge noise.*

- **Preliminary Experiment III:** To validate conjecture III, we conduct experiments on AIR-36 and NREL-PA with various edge deletion probabilities and threshold values  $\epsilon$  using IGNNK. The empirical results are presented in Fig 4. When  $\epsilon$  is 0.1, the MAE of IGNNK decreases under certain edge deletion probabilities for AIR-36 and NREL-PA, indicating the presence of noise. Notably, when  $\epsilon$  is 0.9, the MAE of IGNNK on AIR-36 decreases when the edge deletion probability is 0.1 and 0.4. On NREL-PA, the MAE of IGNNK decreases when the edge deletion probability is between 0.1 and 0.5.

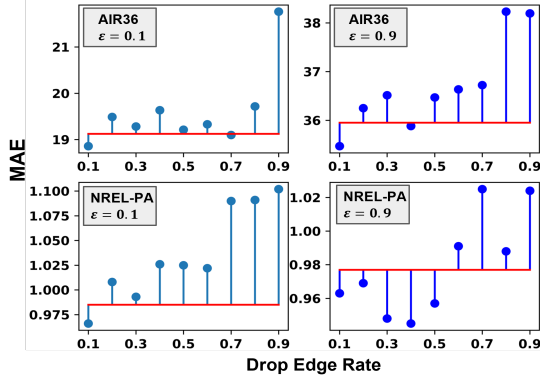


Fig. 4. MAE comparison of IGNNK with different edge-dropping rate and  $\epsilon$  on AIR-36 and NREL-PA. The red horizontal line represents the MAE of the standing IGNNK.

**Observation III:** Even if a larger  $\epsilon$  is used to make the SPGs more sparse, the noise caused by the edges constructed by geographical distance still exists. In other words, noise edges still exist in the SPGs no matter how  $\epsilon$  is selected.

### C. Motivation

Combining the observations in sections §III.B.1 and §III.B.2, it is imperative to develop a framework that can mitigate the shortcomings associated with both PCGs and SPGs. This framework should possess two key features: (1) *the capability to employ topological prompts to counteract potential graph sparsity*, and (2) *a comprehensive noise reduction strategy designed to diminish noise resulting from either excessive graph density or misleading information intrinsic to the edges themselves*.

## IV. METHODOLOGY

### A. DARKFARSEER Overview

1) *Training Protocol:* Recalling the definition from §II, ISK requires predicting  $N_u$  virtual nodes that are not seen during the training phase. Therefore, the key to ISK is to simulate the inference environment during the training phase. The decrement strategy [4] is currently the mainstream training approach for ISK. We thus adopt a decrement training strategy following IGNNK [4]. Specifically, during the training phase, we randomly mask  $N_u$  nodes as the virtual nodes to be predicted and use the subgraph formed by the remaining  $N_o - N_u$  nodes to optimize the kriging model. This subgraph is represented as  $\mathcal{G}_s = (\mathcal{V}_s, \mathcal{E}_s)$ , with  $\mathbf{A}_s \in \mathbb{R}^{(N_o - N_u) \times (N_o - N_u)}$ .

2) *Architecture:* The overall architecture of DARKFARSEER is illustrated in Fig. 5. At its core, DARKFARSEER leverages graph structures and observed node sequences to jointly learn patterns for virtual nodes. It consists of three key components: Style Transfer Embedding (STE), Virtual-Component Contrastive Learning (VCCL), and Similarity-Based Graph Denoising Strategy (SGDS). The STE module comprises the Neighbor Hidden Style Enhancement (NHSE) and a GNN backbone. First, NHSE enhances the temporal styles of the 1-hop neighbors of virtual nodes. Then, a GNN aggregates these enhanced features to predict virtual nodes, as

depicted in Fig. 5(a). VCCL operates on two graph views to compute the contrastive loss  $\mathcal{L}_{VC}$ . It utilizes graph topological information to create prototypes, emphasizing the relationship between virtual node patterns and regional prototype patterns. This mitigates graph sparsity, as illustrated in Fig. 5(b). SGDS reduces graph noise by adjusting edge weights based on the similarity of node sequences and their prototypes. The resulting denoised graph structure,  $A_s^{drop}$ , is shown in Fig. 5(c). Finally, STE re-encodes spatio-temporal patterns using the denoised graph. DARKFARSEER is optimized with a combination of prediction loss  $\mathcal{L}_{MSE}$  and contrastive loss  $\mathcal{L}_{VC}$ . The subsequent sections provide detailed explanations of each module.

### B. Style Transfer Embedding (STE)

We propose a Neighbor Hidden Style Enhancement (NHSE) that performs hidden temporal-style mining on the 1-hop neighbors of *virtual nodes*. We then integrate this module into an existing GNN, forming our STE module. This design aims to organize the T-operator and GNN in a temporal-then-spatial manner, enabling the GNN to transfer the temporal style of neighbors to virtual nodes. Additionally, our NHSE can be seamlessly integrated into existing kriging backbones, improving the performance of kriging tasks.

1) *Neighbor Hidden Style Enhancement (NHSE):* The transition from the training phase to the inference phase for a graph-based ISK model merely involves altering the adjacency matrix from  $\mathbf{A}^o$  to the full  $\mathbf{A}$ . In the inference phase, the model performs temporal knowledge transfer from observed nodes to virtual nodes based on the topological information provided by the full  $\mathbf{A}$ . Hence, constructing topological prompts by utilizing the adjacency relationships between virtual nodes and other nodes is of crucial importance. Correspondingly, the NHSE design mines the temporal style (e.g., seasonality-trends) of virtual node neighbors by leveraging the topological information of their 1-hop neighbors, enabling the GNN to effectively perform style transfer [11], [12] from neighbors to virtual nodes.

Neighbor enhancement needs to be applied to the neighbors of virtual nodes. Since the number of virtual nodes and their neighbors is unknown, a fixed-node approach cannot be used for modeling. The recent discovery of Channel Independence [23] has spurred a plethora of studies that leverage this concept for modeling purposes [24]–[26]. The principle of channel independence seeks to disregard the interdependencies between series, concentrating instead on capturing temporal dependencies within univariate series. Drawing inspiration from channel independence, we introduce DLinear [23], which possesses a powerful ability to decouple trend and seasonal components, to mining the temporal patterns of the neighbors. Let  $\mathcal{N}(i)$  represent the neighbors of the virtual node  $i$ . We first use DLinear to obtain the hidden style sequences  $\mathbf{S}$  of the corresponding series, which is denoted as:

$$\mathbf{S}_j = \sigma(\text{DLinear}(\mathbf{X}_{s,j})), j \in \mathcal{N}(i), i \in \mathcal{V}^u, \quad (8)$$

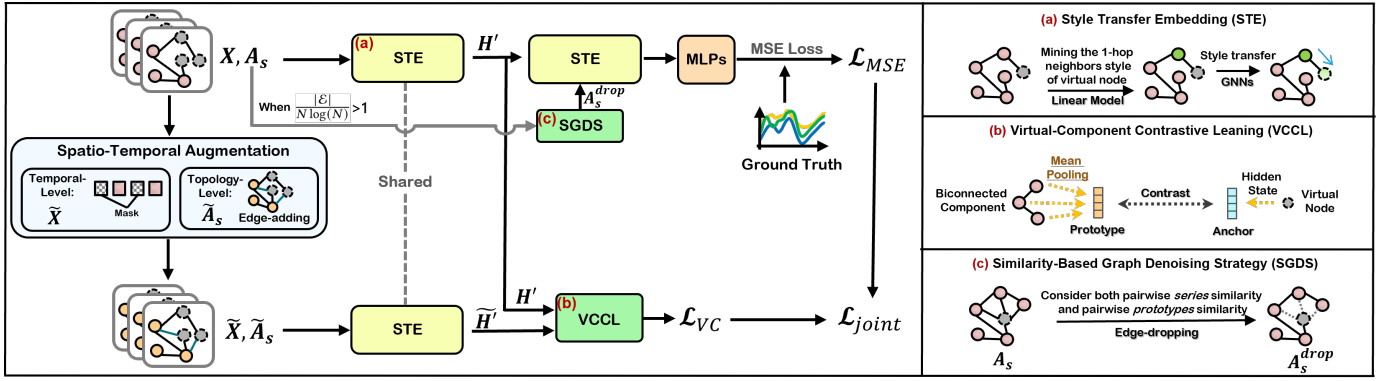


Fig. 5. Overall architecture of DARKFARSEER. At a high level, DARKFARSEER uses graph structures and node sequences to learn patterns for virtual nodes. DARKFARSEER consists of three key components: the STE, VCCL, and SGDS. All of these focus on virtual nodes. (a) STE uses NHSE to mine the temporal style of neighbors and implements temporal style transfer using GNNs. (b) VCCL compares virtual nodes as anchors with the prototypes pooled by BCCs. (c) SGDS performs edge-dropping by considering the feature similarity between virtual nodes and their neighbors.

where  $\sigma(\cdot)$  is the Sigmoid activation function. Subsequently, we fuse this  $\mathbf{S}$  with the corresponding sequence. For simplicity, we use element-wise multiplication for the fusion:

$$\mathbf{H}_j = \mathbf{H}_j \odot \mathbf{S}_j, j \in \mathcal{N}(i), i \in \mathcal{V}^u, \quad (9)$$

where  $\odot$  is the Hadamard product.  $\mathbf{H} \in \mathbb{R}^{(N_o - N_u) \times p \times \varphi}$  is the hidden state, and  $\varphi$  is the hidden dimension.

2) *GNN Backbone*: Our NHSE can be integrated with most existing graph-based backbones [4], [5], [7]–[9], owing to their excellent message-passing mechanisms that aggregate the temporal representations of observed nodes to virtual nodes. We introduce the MPNN [27] as the GNN backbone, which is expressed as:

$$\mathbf{H}' = \text{MPNN}(\mathbf{H}, \mathbf{A}_s), \quad (10)$$

The benefits of performing NHSE are twofold. First, it allows the subsequent GNN to fully learn the representations of virtual nodes. Second, mining the temporal styles of the virtual nodes' neighbors enhances the GNN's robustness when facing graph sparsity and noise. Additionally, the NHSE can be seamlessly integrated into existing graph-based kriging backbones (GNNs), resulting in substantial improvements in ISK performance. We elaborate on this in §V.F.

### C. Virtual-Component Contrastive Learning (VCCL)

In §III.B.1, we discuss the sparsity issue faced by PCGs. Preliminary experiments adding edges between nodes and others in their BCC show this can be mitigated with additional topological cues (**Observation I**). Building on this and the successful application of graph components in some deep learning tasks [13], [28], [29], we design the VCCL to enrich the representation of virtual nodes and address the limitations of sparse graphs. Simply put, we enhance the STE (§IV.B) by using virtual nodes as anchors and the mean pooling of BCC as prototypes [14] to construct their contrast. Additionally, we establish some filtering rules for *false negative samples*.

1) *Temporal and Topological Augmentations*: The general paradigm of CL involves augmenting input data and designing pretext tasks to help the model learn more effective feature

representations. It has achieved significant success in fields like CV [30] and NLP [31]. For ISK tasks, designing augmentations is equally important for CL. We employ existing temporal and Topological augmentation methods for augmentations. *Temporal Augmentation*: Timestamp Masking [32] is a commonly used augmentation method in temporal CL. Specifically, each sequence element within a time window has a probability  $p_t$  of being masked. We set  $p_t = 0.2$ . *Topology Augmentation*: Randomly deleting known edges and adding edges are common methods for topology-level augmentation. Due to the graph sampling required by the decrement training strategy (§IV.A.1), which reduces graph density, we opt for edge-adding as the augmentation method rather than the former. Specifically, if there is no edge between two nodes, there is a probability  $p_s$  of adding an edge. We set  $p_s$  to 0.003.

2) *Contrast Design*: In this part, we explore how to apply the CL paradigm to ISK to accurately model the virtual patterns of virtual nodes. The design of CL involves the selection of three types of objects: anchor, positive samples, and negative samples.

a) *Anchor Selection*: In CL, anchors are used to establish reference points that guide the model to focus on specific features. In the context of time series analysis, the selection of anchors needs to be tailored to the characteristics of the task. Common choices include a time window (or a timestamp) [33], cluster centers [34], or expert knowledge [35]. ISK requires predicting the sequence of virtual nodes based on the sequence of observed nodes. Therefore, the patterns of the virtual nodes is a crucial feature that the ISK model needs to focus on. Recently, the KCP framework constructs Neighboring Contrast and Prototypical Head for ISK. However, using a one-size-fits-all approach by treating all nodes (both observed and virtual) as anchors is not conducive to learning representations specific to the features of virtual nodes and increases modeling complexity. Therefore, we pioneeringly propose using only virtual nodes as anchors.

b) *Biconnected Component (BCC)*: BCCs are subgraphs with high local dependency, capable of representing regional information [28]. Specifically, following [28], we set a threshold  $\mu$ , and only edges with values greater than  $\mu$  are used for

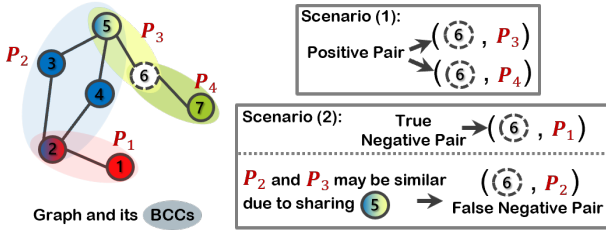


Fig. 6. Illustrations of Scenario (1) and (2).

solving BCC. In other words,  $\mu$  is used to control the sparsity of the BCC. Subsequently, we use the Tarjan algorithm [36], based on depth-first search, to identify the BCCs of the given graph. Mathematically, we represent each node  $i$  in the graph and its corresponding BCC  $C_j$  using  $\{(i, C_j) \mid i \in \mathcal{V}, i \in C_j, j \in \{1, 2, \dots, m\}\}$ , where  $m$  is the number of solved BCCs.

c) *Positive and Negative Samples Selection*: To fully leverage topological prompts, we decide to combine Prototypical Contrastive Learning [14] and BCC. Prototypical Contrastive Learning uses K-Means to select hard cluster centers as prototypes for CL. Inspired by [13], [37], we construct soft cluster centers as prototypes through BCC. Specifically, for each BCC  $C_i$ , we calculate the average hidden state of all nodes within  $C_i$  as the prototype, which can be formalized as:

$$\mathbf{P}_i = \frac{1}{|C_i|} \sum_{j \in C_i} \widetilde{\mathbf{H}}_j, \quad (11)$$

where  $\widetilde{\mathbf{H}}$  is the hidden state of augmented view. In this way, the prototype represented by the mean of the BCC encapsulates the comprehensive features of a regional area. By constructing contrasts between the virtual nodes and these prototypes, we can establish connections between the virtual patterns of the nodes and the regional patterns of BCCs.

However, when constructing this contrast, the following two scenarios should be taken into account: (1) A virtual node (anchor) exists in two or more BCCs; (2) The prototypes of other BCCs corresponding to the remaining nodes in the BCC containing the virtual node cannot be used as negative samples.

For **scenario (1)**, as shown in Fig 6, the virtual node 6 appears in both  $\mathbf{P}_3$  and  $\mathbf{P}_4$ .  $\mathbf{P}_3$  and  $\mathbf{P}_4$  should have similar patterns to node 6, so  $\mathbf{P}_3$  and  $\mathbf{P}_4$  should be considered positive samples. That is, all prototypes corresponding to the BCCs where the virtual node is located should be considered **positive samples**.

For **scenario (2)**, in Fig 6, the virtual node 6 is located in the BCC corresponding to prototype  $\mathbf{P}_3$  (yellow area). This BCC includes node 5, which is also located in the BCC corresponding to  $\mathbf{P}_2$  (blue area). This means node 5 shares part of the pattern of  $\mathbf{P}_3$  and part of the pattern of  $\mathbf{P}_2$ . Thus,  $\mathbf{P}_2$  would become a false negative sample. Therefore, when selecting negative samples, we filter out these types of prototypes to avoid generating *false negative samples*. On the other hand,  $\mathbf{P}_1$  does not share any nodes with  $\mathbf{P}_3$  or  $\mathbf{P}_4$ , so  $\mathbf{P}_1$  can be used as a **negative sample**.

Considering the above two scenarios, the InfoNCE [38] for a single virtual node  $i$  can be expressed as:

$$CL(h_i) = \frac{1}{|P_i^+|} \sum_{\mathbf{p}_k \in P_i^+} -\log \frac{\exp(s(h_i, \mathbf{p}_k)/\tau)}{\exp(s(h_i, \mathbf{p}_k)/\tau) + \sum_{\mathbf{p}_j \in P_i^-} \exp(s(h_i, \mathbf{p}_j)/\tau)}, \quad (12)$$

where  $h_i$  is the hidden state of virtual node  $i$ .  $s(\cdot, \cdot)$  is the cosine similarity function.  $\tau$  is the temperature hyperparameter.  $P_i^+$  is the set of prototypes that should be positive samples (**scenario (1)**) of virtual node  $i$ .  $P_i^-$  is the set of prototypes that should be negative samples (**scenario (2)**) of virtual node  $i$ . The total contrastive loss that the model needs to optimize is:

$$\mathcal{L}_{VC} = \frac{1}{|\mathcal{V}^o|} \sum_{i \in \mathcal{V}^o} CL(h_i). \quad (13)$$

#### D. Similarity-Based Graph Denoising Strategy (SGDS)

Combining **Observation II** and **Observation III**, we motivate the need to design a comprehensive noise reduction strategy to handle the noisy edges present in dense PCGs and SPGs. In this section, we design a simple yet effective graph denoising strategy for ISK.

Structure noise in GNNs refers to the presence of irrelevant or noisy information in the graph structure that can negatively impact the performance of the GNN model [39]. GNNs are highly susceptible to structure noise since errors can propagate throughout the graph due to the message-passing mechanism [40]. Therefore, the quality of the input graph structure is critical to achieving optimal GNN performance. Inspired by Robust Graph Neural Networks [41]–[44], we design the SGDS, which aims at optimizing graph structures and reducing the interference of noisy edges to enhance the robustness of ISK models. Given the specific nature of ISK, we focus on handling edges related to virtual nodes. Specifically, for each virtual node  $i \in \mathcal{V}^u$ , we assess the sequence similarity and prototype (§IV.C) similarity between it and each of its neighboring nodes  $j \in \mathcal{N}(i)$ , obtaining the weighted similarity  $\gamma_{i,j}$ :

$$\gamma_{i,j} = \alpha s(\mathbf{P}_i, \mathbf{P}_j) + (1 - \alpha) s(\mathbf{H}'_i, \mathbf{H}'_j), \quad (14)$$

where  $\alpha = \frac{1}{\mathcal{D}}$  controls the proportion of different similarities, and  $\mathcal{D} = \frac{|\mathcal{E}|}{N \log(N)}$  is used to measure the sparsity of the graph. This setup aims to consider prototype similarity more when the graph is sparse, and node feature similarity more when the graph is dense, to assess the importance of hidden edges. Subsequently, we select the Bottom- $K$  lowest  $\gamma$  values, representing the weakest connections, and set the corresponding edges in  $\mathbf{A}_s$  to  $\omega$ , getting the  $\mathbf{A}_s^{drop}$ :

$$\mathbf{A}_{s, i, j} = \omega, \quad (15)$$

where  $\omega$  is a low-intensity value. The value of  $K$  corresponding to virtual node  $i$  is  $\lfloor |\mathcal{N}(i)| \times \beta \rfloor$ , where  $\beta$  is the probability of edge dropping, with  $0 < \beta < 1$ .  $i$  and  $j$  correspond to the indices of the two nodes in the Bottom- $K$   $\gamma$ . This approach aims to balance fine-grained temporal pattern similarity and regional pattern similarity between nodes, thereby optimizing edge selection and improving the overall quality of the graph. For the ISK task, since  $\mathbf{A}$  is denser during the inference phase

compared to  $\mathbf{A}_s$  during the training phase, we set  $\beta$  to 1.2 times the value used during inference. Additionally, to enable DARKFARSEER to adaptively apply SGDS, we set the SGDS module to activate only when  $\mathcal{D} > 1$ .

### E. Loss Function

Unlike previous works [4] that reconstruct all nodes to train the ISK model, to allow DARKFARSEER to focus on virtual nodes, we train using a randomly selected sequence of  $V^u$  nodes while optimizing both the MSE (Mean Squared Error) loss and the contrastive loss  $\mathcal{L}_{VC}$ :

$$\mathcal{L}_{joint} = \frac{1}{|\mathcal{V}^u|p} \sum_{i \in \mathcal{V}^u} \sum_{t=1}^p (x_{i,t}^o - \hat{x}_{i,t})^2 + \eta \mathcal{L}_{VC}, \quad (16)$$

where  $\eta$  is the weight coefficient for the contrastive loss  $\mathcal{L}_{VC}$ .

### F. Complexity Analysis

1) *Time Complexity*: For NHSE, the time complexity of Equation 8 is  $\mathcal{O}(p)$ , and Equation 9 is implemented using a mask, resulting in a time complexity of  $\mathcal{O}(1)$ . Therefore, the total time complexity of NHSE is  $\mathcal{O}(p) + \mathcal{O}(1) = \mathcal{O}(p)$ . During the training phase, for VCCL, calculating the prototypes for positive and negative samples for each virtual node incurs a cost of  $\mathcal{O}(mN_u)$ , assuming each BCC is utilized. Computing the  $\mathcal{L}_{VC}$  for  $N_u$  virtual nodes requires  $\mathcal{O}(N_u)$ . Therefore, the overall time complexity of VCCL is  $\mathcal{O}(mN_u) + \mathcal{O}(N_u) = \mathcal{O}(mN_u)$ . For SGDS, assuming that the average degree of nodes is  $d$  and ignoring the complexity of calculating the Bottom-K, it requires  $\mathcal{O}(dN_u)$ . In summary, disregarding the GNN, the time complexities of DARKFARSEER during the training and inference phases are  $\mathcal{O}(p + (m + d)N_u)$  and  $\mathcal{O}(p + dN_u)$ , respectively.

2) *Space Complexity*: For DARKFARSEER, a batch of sequences is input with the shape  $[B, \varphi, N', p]$ , where  $B$  represents the batch size and  $N'$  is the number of neighboring nodes corresponding to the virtual nodes. NHSE utilizes DLinear (Equation 8) consuming memory  $\mathcal{O}(B\varphi N'p)$ . In VCCL and SGDS, obtaining the prototype of a BCC using mean pooling incurs a cost of  $\mathcal{O}(B\varphi p)$ . In VCCL, computing the InfoNCE loss requires  $\mathcal{O}(B\varphi p)$  in Equation 12. In SGDS, calculating  $\gamma$  requires  $\mathcal{O}(B\varphi p)$  in Equation 14. Therefore, disregarding the GNN, the overall space complexity of DARKFARSEER during the training and inference phases is  $\mathcal{O}(B\varphi N'p + B\varphi p)$ .

**Remark.** Noting that  $N_u$  and  $N'$  are smaller than  $N$  and have a linear relationship with  $N$ , therefore, as  $N$  increases (i.e., for larger graphs), the time and space complexities of DARKFARSEER do not grow exponentially, indicating that DARKFARSEER is scalable.

## V. EXPERIMENTS AND RESULTS

We provide empirical results to demonstrate the effectiveness of our proposed DARKFARSEER model. The experiments are designed to answer the following research questions: (i) **RQ1** How does DARKFARSEER perform on multiple datasets, compared to the SOTA ISK models? (ii) **RQ2** Are the designs of each component in DARKFARSEER effective? (iii) **RQ3**

Can the functions of VCCL and SGDS be elucidated through qualitative analysis? (iv) **RQ4** Is DARKFARSEER robust to different distributions of virtual nodes? (v) **RQ5** Can the NHSE module enhance different kriging backbones? (vi) **RQ6** How do important parameters affect DARKFARSEER? Is DARKFARSEER sensitive to them?

TABLE III  
THE OVERALL INFORMATION FOR DATASETS.

Datasets	Traffic Flow		Traffic Speed	Air Quality	Solar Power
	PEMS03	PEMS04	PEMS-BAY	AIR-36	NREL-PA
Region	California		San Francisco	Beijing	Pennsylvania
Graph type	Pairwise Connectivity Graphs			Spatial Proximity Graphs	
Nodes	358	307	325	36	101
Timesteps	26,208	16,992	52,128	8,759	105,120
Interval	5min	5min	5min	1hour	5min
Start time	9/1/2018	1/1/2018	1/1/2017	5/1/2014	1/1/2006

### A. Experiment Setup

1) *Datasets*: We validate our proposed method on five real-world datasets across four different scenarios: traffic flow, traffic speed, air quality, and solar power. Detailed information about the datasets is shown in TABLE III.

- **PEMS03**<sup>1</sup>: The dataset includes data from multiple traffic sensors located along the I-880 highway in California.
- **PEMS04**<sup>1</sup>: The dataset includes data from multiple traffic monitoring sensors located on specific highway networks in California, primarily along the I-105 and SR-73 highways. We only consider the traffic flow output from PEMS03 and PEMS04.
- **PEMS-BAY**<sup>2</sup>: The dataset comprises data from numerous traffic sensors strategically positioned across the San Francisco Bay Area’s extensive highway network.
- **AIR-36**<sup>3</sup>: The dataset is a specialized subset focused on air quality research. We consider only the PM2.5 pollutant.
- **NREL-PA**<sup>4</sup>: The dataset records the solar power outputted by 101 photovoltaic power plants in Pennsylvania in 2006.

2) *Baselines*: We compare DARKFARSEER with following baselines:

- **MEAN**: At fixed timestamps, we use the mean of each observed node in the test set to fill virtual nodes.
- **KNN**: K-Nearest Neighbors fills virtual nodes by using the average of the  $K$  nearest observed nodes. We set  $K = 10$ .
- **SATCN** [45]: SATCN captures diverse information from a node’s neighbors through multiple aggregation functions.
- **IGNNK** [4]: A graph-based ISK model employs a three-layer Graph Diffusion Layer with residual connections.
- **DualSTN** [9]: In both long-term and short-term modes, pattern learning is performed using graph and attention.
- **INCREASE** [6]: INCREASE aggregates the heterogeneous spatial information of K-nearest neighbors to perform ISK.
- **KCP** [7]: A graph-based CL framework for ISK. It constructs spatial contrast and temporal heterogeneity contrast through neighbor comparisons and Prototype Heads.

<sup>1</sup><https://github.com/Davidham3/STSGCN/>

<sup>2</sup><https://github.com/liyaguang/DCRNN>

<sup>3</sup><https://github.com/Graph-Machine-Learning-Group/grin>

<sup>4</sup><https://www.nrel.gov/grid/solar-power-data.html>



TABLE IV

PERFORMANCE COMPARISON OF INDUCTIVE SPATIO-TEMPORAL KRIGING OVER FIVE DATASETS, WITH THE RESULTS REPORTED AS MEAN $\pm$ STD. THE TOP AND SECOND-BEST RESULTS ARE EMPHASIZED IN **BOLD** AND UNDERLINED TEXT. N/A DENOTES THE RESULTS COULD NOT BE OBTAINED SINCE THE AUGMENTATION METHODS PROVIDED IN KCP [7] DO NOT WORK ON PEMS-BAY.

Datasets	Metrics	MEAN	KNN	SATCN	IGNNK	DualSTN	INCREASE	KCP	Ours	Improv
PEMS03	MAE	79.780	94.804	25.985 $\pm$ 0.300	<u>19.660<math>\pm</math>0.277</u>	23.971 $\pm$ 0.266	22.707 $\pm$ 1.416	25.106 $\pm$ 0.009	<b>17.908<math>\pm</math>0.077</b>	8.91%
	RMSE	101.791	114.96	43.812 $\pm$ 0.438	<u>29.573<math>\pm</math>0.285</u>	34.917 $\pm$ 0.593	36.417 $\pm$ 0.781	40.123 $\pm$ 0.010	<b>27.532<math>\pm</math>0.267</b>	6.90%
	MRE	0.457	0.977	0.348 $\pm$ 0.005	<u>0.117<math>\pm</math>0.001</u>	0.143 $\pm$ 0.003	0.135 $\pm$ 0.008	0.150 $\pm$ 0.000	<b>0.107<math>\pm</math>0.000</b>	8.54%
PEMS04	MAE	89.241	91.036	53.682 $\pm$ 0.981	<u>34.700<math>\pm</math>0.171</u>	37.433 $\pm$ 0.571	42.089 $\pm$ 0.666	44.704 $\pm$ 0.113	<b>31.026<math>\pm</math>0.110</b>	10.58%
	RMSE	116.288	110.426	76.786 $\pm$ 1.340	<u>52.632<math>\pm</math>0.260</u>	55.806 $\pm$ 0.745	63.103 $\pm$ 0.537	66.783 $\pm$ 0.110	<b>47.137<math>\pm</math>0.155</b>	10.44%
	MRE	0.406	0.443	0.690 $\pm$ 0.032	<u>0.165<math>\pm</math>0.000</u>	0.178 $\pm$ 0.002	0.199 $\pm$ 0.003	0.212 $\pm$ 0.005	<b>0.147<math>\pm</math>0.000</b>	10.90%
PEMS-BAY	MAE	4.694	4.947	3.126 $\pm$ 0.300	<u>2.769<math>\pm</math>0.036</u>	2.975 $\pm$ 0.033	2.786 $\pm$ 0.061	N/A	<b>2.697<math>\pm</math>0.027</b>	2.60%
	RMSE	7.882	8.070	6.114 $\pm$ 0.049	<u>5.265<math>\pm</math>0.048</u>	5.544 $\pm$ 0.042	5.488 $\pm$ 0.038	N/A	<b>5.148<math>\pm</math>0.024</b>	2.22%
	MRE	0.075	0.079	0.067 $\pm$ 0.000	<u>0.044<math>\pm</math>0.000</u>	0.047 $\pm$ 0.000	0.044 $\pm$ 0.000	N/A	<b>0.043<math>\pm</math>0.000</b>	2.27%
AIR-36	MAE	19.499	20.696	20.099 $\pm$ 3.638	<u>19.124<math>\pm</math>0.350</u>	25.674 $\pm$ 1.291	16.969 $\pm$ 1.034	22.556 $\pm$ 0.169	<b>15.382<math>\pm</math>0.200</b>	9.35%
	RMSE	31.902	32.256	30.705 $\pm$ 3.898	<u>29.279<math>\pm</math>0.339</u>	38.367 $\pm$ 1.823	<u>26.829<math>\pm</math>0.475</u>	34.937 $\pm$ 0.460	<b>26.293<math>\pm</math>0.223</b>	1.99%
	MRE	0.229	0.277	0.604 $\pm$ 0.118	<u>0.230<math>\pm</math>0.004</u>	0.309 $\pm$ 0.015	<u>0.204<math>\pm</math>0.012</u>	0.272 $\pm$ 0.001	<b>0.185<math>\pm</math>0.002</b>	9.31%
NREL-PA	MAE	0.937	0.944	1.622 $\pm$ 0.078	<u>0.977<math>\pm</math>0.036</u>	0.998 $\pm$ 0.013	1.420 $\pm$ 0.203	1.289 $\pm$ 0.058	<b>0.888<math>\pm</math>0.015</b>	5.22%
	RMSE	2.073	2.053	2.313 $\pm$ 0.078	<b>1.545<math>\pm</math>0.037</b>	1.596 $\pm$ 0.018	2.029 $\pm$ 0.225	1.891 $\pm$ 0.017	1.555 $\pm$ 0.008	-
	MRE	0.401	0.589	0.229 $\pm$ 0.007	<u>0.228<math>\pm</math>0.008</u>	0.233 $\pm$ 0.003	<u>0.215<math>\pm</math>0.003</u>	0.301 $\pm$ 0.013	<b>0.208<math>\pm</math>0.003</b>	3.25%

### 3) Implementation Details: Evaluation Configuration:

Unless otherwise specified, we set the random seed to 0 (of *numpy* library), with an observed-to-virtual nodes ratio of 3:1. The dataset is split into training, validation, and test sets in a ratio of 6:2:2. Experiments are conducted four times, and the results are averaged. The time window  $p$  is set to 24. We normalize the training and validation sets using the values from the observed nodes in the training set, and each node in the test set is normalized individually. The Adam optimizer is used for optimization with a fixed learning rate of 0.0005. The batch size is set to 32, the number of training epochs to 300, and gradient clipping is 5.0. The adjacency matrices constructed for all datasets are normalized using Equation 7, where  $\varepsilon$  is set to  $+\infty$  for PEMS03, PEMS04 and PEMS-BAY, and to 0.1 for AIR-36 and NREL-PA. We use Mean Absolute Error (MAE), Root Mean Square Error (RMSE), and Mean Relative Error (MRE) [27], [46] as evaluation metrics. Lower values of these metrics indicate better model performance. **Model Parameters:** We set the hidden dimension  $\varphi$  to 64. For the five datasets (PEMS03, PEMS04, PEMS-BAY, AIR-36 and NREL-PA),  $\mu$  is set to  $\{0.0, 0.0, 0.7, 0.85, 0.7\}$  and  $\eta$  is set to  $\{0.07, 0.07, 0.007, 0.01, 0.001\}$ . The edge dropout rate  $\beta$  is set to 0.1.  $\omega$  sets to 0.01. **Experimental Environment:** Our code is implemented using Python 3.10.9 and PyTorch 2.2.1. All experiments are conducted on an NVIDIA GeForce RTX 4090 GPU, a 12th Gen Intel(R) Core(TM) i9-12900K CPU, and Ubuntu 20.04.6 LTS.

### B. Performance Comparison (RQ1)

To answer **RQ1**, we conduct comparative experiments with seven baselines across five real-world datasets from different domains, as shown in TABLE IV. DARKFARSEER achieves the best performance on four of these datasets, excluding the RMSE of NREL-PA. This fully demonstrates DARKFARSEER’s strong generalization capability across datasets from different domains. For the graph-sparse traffic flow datasets PEMS03 and PEMS04, DARKFARSEER outperform the second-best baseline, IGNNK, in MAE, RMSE, and MRE,

and significantly exceeded other baselines. This is attributed to VCCL’s ability to enrich virtual node representations by constructing contrasts between virtual nodes and graph components, thereby alleviating graph sparsity. Although IGNNK achieve excellent performance, its three-layer GNN is unable to capture sufficient information on sparse graphs, leading to suboptimal results. For the graph-dense traffic speed datasets PEMS-BAY, DARKFARSEER achieve SOTA performance. This success can be attributed to DARKFARSEER’s SGDS, which effectively denoises dense graphs, allowing the GNN to model the virtual nodes on low-noise graph structures. On PEMS-BAY, INCREASE is second-best in MAE and MRE compared to our model, possibly because INCREASE focuses on k-nearest neighbors and thus overlooks global information. On the SPGs graphs AIR-36 and NREL-PA, SPGs are approximated based on geographic distances, which introduces noise (§III.B.2). DARKFARSEER, equip with SGDS, benefits from its denoising capabilities, outperforming the second-best model in MAE and MRE. On AIR-36, although INCREASE achieve excellent performance, the simplistic k-nearest neighbors aggregation struggled to differentiate noise, resulting in suboptimal outcomes. On NREL-PA, DARKFARSEER’s RMSE is slightly worse than that of IGNNK. This may be due to the presence of outliers in NREL-PA, which makes DARKFARSEER’s SGDS module struggle. MEAN secure the second-best MAE, likely because excessive graph noise obscured node interactions. Aside from DARKFARSEER, other methods find it challenging to accurately distinguish these node details.

### C. Ablation Study (RQ2)

To study **RQ2**, we perform an ablation study on PEMS04, PEMS-BAY, and NREL-PA. Results for the other two datasets are available in the supplementary materials. Specifically, we design a set of DARKFARSEER variants and observe the effects of different variants on MAE, RMSE, and MRE. For clarity, we name the variants as follows:

- DARKFARSEER-B: Only a two-layer MPNN is used.

TABLE V  
ABLATION ON PEMS04, PEMS-BAY AND NREL-PA.

Variants @PEMS04	MAE	RMSE	MRE
DARKFARSEER-B	37.063±0.345	56.944±0.198	0.176±0.001
DARKFARSEER-N	31.483±0.226	47.680±0.180	0.149±0.001
DARKFARSEER-CL	<b>31.026±0.110</b>	<b>47.137±0.155</b>	<b>0.147±0.000</b>
Variants @PEMS-BAY	MAE	RMSE	MRE
DARKFARSEER-B	2.803±0.035	5.312±0.081	0.044±0.000
DARKFARSEER-N	2.757±0.031	5.270±0.067	0.044±0.000
DARKFARSEER-CL	2.771±0.040	5.263±0.018	0.044±0.000
DARKFARSEER-D	<b>2.697±0.027</b>	<b>5.148±0.024</b>	<b>0.043±0.000</b>
Variants @NREL-PA	MAE	RMSE	MRE
DARKFARSEER-B	0.912±0.032	<b>1.540±0.004</b>	0.213±0.007
DARKFARSEER-N	0.908±0.044	1.542±0.017	0.212±0.010
DARKFARSEER-CL	0.898±0.030	1.544±0.007	0.210±0.007
DARKFARSEER-D	<b>0.888±0.015</b>	1.555±0.008	<b>0.208±0.003</b>

- DARKFARSEER-N: On top of DARKFARSEER-B, NHSE is added before the MPNN.
- DARKFARSEER-CL: VCCL is added on top of DARKFARSEER-N.
- DARKFARSEER-D: SGDS is activated on top of DARKFARSEER-CL.

The experimental results are reported in TABLE V. Note that, since SGDS is not activated on PEMS04, we do not explore the results of DARKFARSEER-D on PEMS04. By comparing DARKFARSEER-B and DARKFARSEER-N, we can observe that NHSE provides considerable improvements to the model across all three datasets, thanks to NHSE’s temporal modeling. Comparing DARKFARSEER-N and DARKFARSEER-CL, we observe that MAE, RMSE, and MRE are significantly reduced on PEMS04 and NREL-PA. However, on PEMS-BAY, MAE does not decrease, which may be due to the fact that for dense PCGs, introducing additional topological information causes the model to struggle. Additionally, compared to DARKFARSEER-CL, DARKFARSEER-D shows reductions in metrics on PEMS-BAY, reflecting the denoising effectiveness introduced by SGDS. For NREL-PA, MAE and MRE decreased, while RMSE increased. This may be attributed to the model becoming more sensitive to errors after using SGDS.

#### D. Interpretability Study (RQ3)

To explore RQ3, we conduct qualitative analyses on both PEMS04 and PEMS-BAY. To determine whether VCCL can provide additional prompts to enrich virtual node representation, we conduct a clustering analysis. Specifically, we cluster the prototypes corresponding to the BCCs of the graph constructed from PEMS04 and examine the proximity of the embeddings associated with the virtual nodes to these cluster centers. We select two virtual nodes with indices 256 and 5 in PEMS04 and visualize the embeddings of these two virtual nodes from DARKFARSEER and IGNNK, as shown in Fig 7. By observing the content within the blue box, we find that the embeddings of the virtual nodes learned by DARKFARSEER are closer to the cluster centers, whereas those of IGNNK are farther from the cluster centers. This

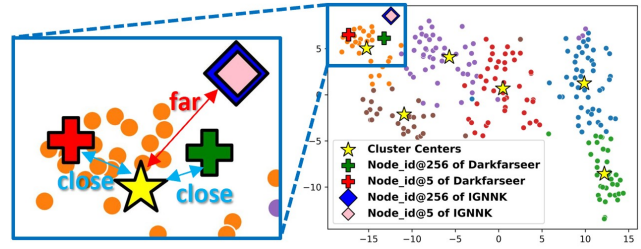


Fig. 7. A qualitative study on PEMS04. We visualize the embeddings of the pooled prototypes and virtual nodes and observe that the virtual nodes encoded by DarkFarseer are closer to the cluster centers compared to those in IGNNK.

indicates that VCCL successfully enabled DARKFARSEER to learn certain topological prompts.

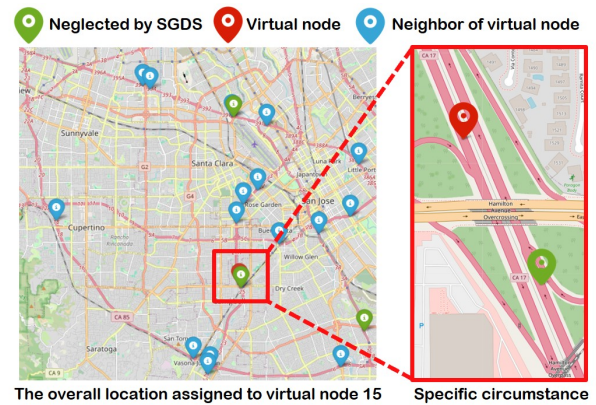


Fig. 8. A qualitative study on PEMS-BAY. We visualize the geographic distribution of virtual node 15 and its neighbors in the real world, with green pins representing neighbors neglected by SGDS. Observing the content within the red box, a neighbor very close to the virtual node is ignored by SGDS. This reflects the characteristics of noisy edges, where spatial proximity does not imply stronger relevance.

To explain SGDS, we visualize the distribution of different nodes in the real world. Fig 8 illustrates the geographical distribution of virtual node 15 (red pin), its retained neighbors (blue pins), and neighbors ignored by SGDS (green pins) in the test set. It can be observe that the green pins are not all the farthest from the red pins, which indicates that distance and the degree of correlation are not directly related [7]. Specifically, as shown in the red box in Fig 8, although the red pin and the green pin are close to each other, there are no reachable roads within the nearby area. This demonstrates their lack of correlation and also explains the rationale behind SGDS’s processing.

#### E. Error Bars Evaluation (RQ4)

The random seed determines the distribution of virtual nodes on the graphs. In other words, the choice of different random seeds results in different virtual nodes being used for inference. Comparing performance across various random seeds better reflects the model’s stability and robustness. To approach RQ4, we compare DARKFARSEER with other deep learning-based ISK methods using random seeds 1 and

TABLE VI

ERROR BARS OF DEEP LEARNING-BASED ISK METHODS WITH TWO DIFFERENT RANDOM SEEDS ON THREE DATASETS. N/A DENOTES THE RESULTS COULD NOT BE OBTAINED SINCE THE AUGMENTATION METHODS PROVIDED IN KCP [7] DO NOT WORK ON PEMS-BAY.

Method	PEMS04@seed 1		PEMS-BAY@seed 1		NREL-PA@seed 1		PEMS04@seed 2		PEMS-BAY@seed 2		NREL-PA@seed 2	
	MAE	RMSE	MAE	RMSE	MAE	RMSE	MAE	RMSE	MAE	RMSE	MAE	RMSE
SATCN	52.940±0.854	74.046±0.832	2.898±0.008	5.431±0.021	1.666±0.025	2.402±0.010	56.237±1.141	78.517±1.352	2.761±0.003	5.217±0.021	1.736±0.055	2.466±0.055
IGNNK	32.191±0.286	48.800±0.397	2.737±0.041	4.876±0.059	0.977±0.012	1.573±0.006	32.862±0.374	47.882±0.297	2.545±0.051	4.641±0.057	1.049±0.008	1.680±0.003
DualSTN	36.024±0.401	53.645±0.544	2.829±0.018	5.067±0.045	0.955±0.024	1.572±0.015	35.216±0.299	51.018±0.338	2.730±0.101	4.978±0.166	1.036±0.015	1.661±0.008
INCREASE	35.416±1.668	53.292±1.024	2.843±0.208	5.479±0.720	1.430±0.043	2.034±0.047	40.621±1.694	61.631±0.827	2.567±0.070	4.814±0.067	1.425±0.070	1.793±0.533
KCP	41.302±0.024	64.685±0.025	N/A	N/A	1.284±0.058	1.965±0.084	43.256±0.020	66.672±0.008	N/A	N/A	1.768±0.024	2.635±0.071
Ours	<b>30.691±0.284</b>	<b>46.597±0.196</b>	<b>2.684±0.026</b>	<b>4.859±0.047</b>	<b>0.896±0.032</b>	<b>1.568±0.020</b>	<b>31.177±0.554</b>	<b>45.540±0.549</b>	<b>2.482±0.008</b>	<b>4.612±0.009</b>	<b>0.979±0.023</b>	<b>1.655±0.008</b>
Improv	<b>4.65%</b>	<b>4.51%</b>	<b>1.93%</b>	<b>0.34%</b>	<b>6.17%</b>	<b>0.25%</b>	<b>5.12%</b>	<b>4.89%</b>	<b>2.47%</b>	<b>0.62%</b>	<b>5.50%</b>	<b>0.36%</b>

2, as shown in TABLE VI. To keep it brief, we present results for three datasets here. For full results, please see the supplementary materials. It can be observed that under two different seeds, DARKFARSEER still outperforms other ISK models, which indicates that DARKFARSEER has good robustness to virtual nodes with different distributions.

TABLE VII

PERFORMANCE OF NHSE WITH MULTIPLE KRIGING BACKBONES.

Variants	PEMS03		PEMS04		AIR-36		PEMS-BAY	
	MAE	RMSE	MAE	RMSE	MAE	RMSE	MAE	RMSE
GD	23.263	35.390	51.514	75.331	21.765	34.099	3.984	7.209
GD w/ NHSE	<b>21.481</b>	<b>32.243</b>	<b>39.663</b>	<b>57.987</b>	<b>20.720</b>	<b>32.482</b>	<b>3.934</b>	<b>7.059</b>
Improv	<b>7.66%</b>	<b>8.89%</b>	<b>23.01%</b>	<b>23.02%</b>	<b>4.80%</b>	<b>4.74%</b>	<b>1.25%</b>	<b>2.08%</b>
GAT	23.134	35.393	41.520	61.105	20.087	29.887	2.894	5.434
GAT w/ NHSE	<b>20.554</b>	<b>30.663</b>	<b>37.185</b>	<b>53.517</b>	<b>19.244</b>	<b>29.580</b>	2.904	5.445
Improv	<b>11.15%</b>	<b>13.36%</b>	<b>10.44%</b>	<b>12.41%</b>	<b>4.19%</b>	<b>1.02%</b>	-	-
MPNN	37.885	52.375	57.342	77.215	19.502	30.250	3.449	6.318
MPNN w/ NHSE	<b>21.017</b>	<b>31.392</b>	<b>34.562</b>	<b>51.347</b>	<b>18.333</b>	<b>28.764</b>	<b>3.244</b>	<b>6.006</b>
Improv	<b>44.52%</b>	<b>40.06%</b>	<b>39.72%</b>	<b>33.50%</b>	<b>5.99%</b>	<b>4.91%</b>	<b>5.94%</b>	<b>4.93%</b>

F. NHSE with Various Kriging Backbones (RQ5)

To examine RQ5, we conduct a study on four datasets by combining three GNN applied to kriging tasks: Graph Diffusion (GD) [4], Graph Attention (GAT) [8], and MPNN [5] integrated with NHSE. The results are reported in TABLE VII, where "w/ NHSE" denotes the corresponding GNN variants integrated with NHSE. Thanks to the integration approach of style transfer strategy and the modeling strategy for virtual nodes, NHSE can generally provide significant improvements to existing graph-based ISK GNN backbones. In particular, for the sparsely connected datasets PEMS03 and PEMS04, the enhancements brought by NHSE are most notable, with improvements reaching 30 to 40 percent on MPNN. This indicates that NHSE enables GNNs to more effectively aggregate neighbor features, thereby alleviating graph sparsity. For the noisy datasets AIR-36 and PEMS-BAY, NHSE consistently yields improvements of 1 to 5 percent. This suggests that NHSE allows GNNs to better distinguish neighbor features, addressing graph noise. Notably, in PEMS-BAY, NHSE did not provide benefits to GAT, which may be due to overfitting when applying NHSE to GATs that utilize attention mechanisms on PEMS-BAY, where the number of neighbors is excessively large.

G. Parameter Study (RQ6)

To investigate RQ6, we conduct parameter studies on the key parameters of our proposed VCCL and SGDS using

the PEMS04, PEMS-BAY, and NREL-PA datasets, where PEMS04 and PEMS-BAY are representative of sparse PCGs and dense PCGs (§III.B.1), respectively, and NREL-PA is representative of SPGs (§III.B.2). We summarize the results in Fig 9. Due to space constraints, only three datasets are presented here. Please refer to the supplementary materials for the parameter study of the remaining datasets.

1) *Impact of BCC's sparsity  $\mu$* :  $\mu$  determines the sparsity of BCCs, and the value of  $\mu$  directly affects the performance of VCCL. For dense graphs, we require more dispersed (sparse) BCCs, whereas for sparse graphs, we need denser BCCs. Therefore, for PEMS04, we perform a grid search for the optimal  $\mu$  between 0.0 and 0.5, while for PEMS-BAY and NREL-PA, we search over larger  $\mu$ . Fig 9(a) presents the results of  $\mu$  in relation to MAE and RMSE. As  $\mu$  increases, both MAE and RMSE on the PEMS04 dataset exhibit an upward trend. This indicates that higher values of  $\mu$  (i.e., sparser BCCs) lead to deteriorated model performance, suggesting that denser BCCs are more suitable for PEMS04 because they provide more topological cues for ISK learning on sparse graphs, aligning with the design philosophy (§III.C) of VCCL. On PEMS-BAY, as  $\mu$  increases, both MAE and RMSE continuously decrease. This indicates that for dense PCGs, a sparser BCC allows VCCL to fully leverage its capabilities. For NREL-PA, DARKFARSEER is not sensitive to MAE, while RMSE increases as  $\mu$  increases. This may be due to the inherent noise in SPGs, and the topological cues provided by a dense BCC configuration for VCCL can help mitigate this.

2) *Impact of VCCL weight  $\eta$* :  $\eta$  determines the weight of VCCL in the total training loss. We perform a grid search for  $\eta$  within a range where its value is either of the same order of magnitude as the MSE loss or one order of magnitude smaller. Fig 9(c) reports the results. Overall, across these three datasets, as  $\eta$  varies, DARKFARSEER's MAE and RMSE fluctuate minimally. This indicates that DARKFARSEER is insensitive to the selection of  $\eta$ .

3) *Impact of drop edge rate  $\beta$* :  $\beta$  determines the proportion of edges from the virtual node that are downgraded in SGDS. Note that, because PEMS04 comprises sparse PCGs ( $D < 1$ ), we do not investigate the use of SGDS on PEMS04. Fig 9(b) and Fig 9(d) report the corresponding MAE and RMSE for PEMS-BAY and NREL-PA. Overall, it can be observed that as  $\beta$  increases, both MAE and RMSE show a significant upward trend. This aligns with the intuition that neglecting too many edges leads to a decline in the performance of DARKFARSEER, which relies on GNNs.

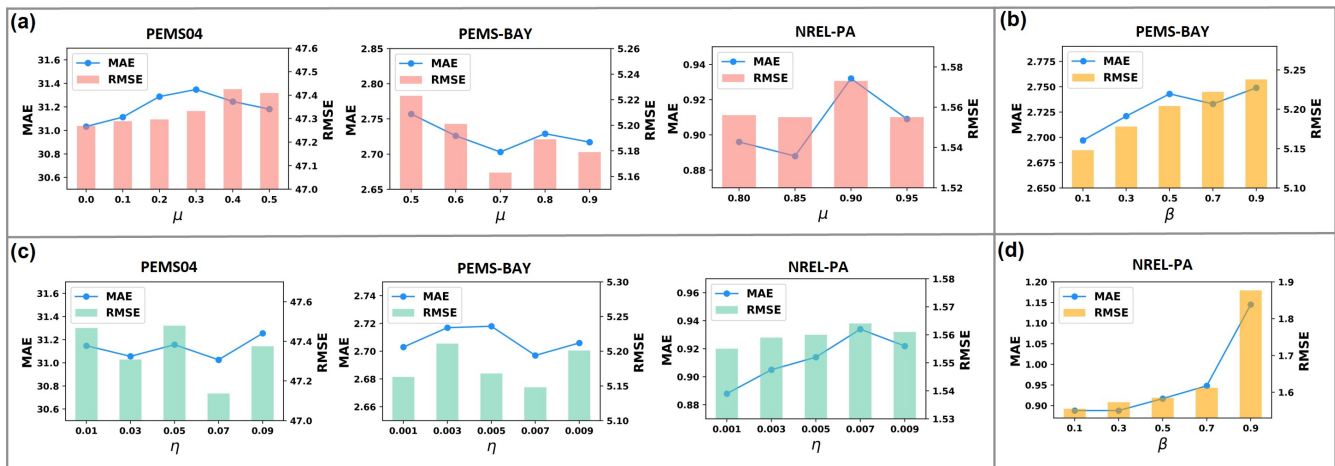


Fig. 9. Parameter study on PEMS04, PEMS-BAY and NREL-PA.

## VI. RELATED WORK

### A. Spatio-temporal Kriging

Kriging is a prominent geostatistical method used for spatial interpolation. Spatio-temporal kriging extends this technique to include the temporal dimension, enabling the estimation of values at unobserved locations at different times [5]. Spatio-temporal kriging is broadly classified into transductive and inductive approaches. Transductive models require all nodes to be available during the training phase and are unable to naturally generate representations for new (virtual) nodes without retraining. Early spatio-temporal kriging methods were often represented by transductive approaches, such as those based on matrix factorization [47]–[49] and graph-based approaches [50]. Although these works have achieved certain successes, TSK is difficult to extend to new nodes. Compared to TSK, inductive models are capable of handling new nodes introduced after training, making them more practical. ISK has recently sparked a wave of research [4], [5], [7]–[9], [51]. The key to ISK lies in transferring temporal patterns from observed nodes to virtual nodes. Deep learning-based ISK methods can be broadly categorized into two paradigms according to the scale of transfer: **partial transfer** and **global transfer**. Global transfer aims to migrate the temporal patterns of all nodes to virtual nodes. The most representative approaches employ GNNs. For example, IGNNK [4] uses Graph Diffusion Layers [52], and KCP [7] utilizes GraphSAGE [53]. Currently, the vast majority of methods rely on global transfer. Partial transfer generally involves migrating based on the k-nearest neighbors of virtual nodes. For instance, INCREASE [6] aggregates and transfers information from heterogeneous k-neighbors specific to a given virtual node. Additionally, the quality of the graph structure significantly affects the effectiveness of graph-based ISK, yet few works have addressed the issue of graph structure quality.

### B. Graph Modeling for Time Series

Since the variable dimensions of multivariate time series (MTS) can often be represented as graphs, the application of

graph representation learning techniques to MTS analysis has become quite prevalent. Different types of graphs applied to MTS can facilitate the learning of varied inductive biases. For instance, the introduction of dynamic graphs allows models to learn time-varying spatial relationships [54]–[57]. Incorporating hypergraphs enables the learning of more complex and intertwined many-to-many spatial relationships [58]–[60]. Thanks to its simple and effective design paradigm, some studies employ contrastive learning to enhance graph learning for time series [61], [62].

### C. Comparison to Existing Approaches

DARKFARSEER is specifically designed to focus on graph modeling tailored for virtual nodes. This strategic focus aims to integrate and leverage the advantages offered by both partial transfer and global transfer. Additionally, the key modules of DARKFARSEER, namely VCCL and SGDS, have been meticulously developed to significantly enhance the model’s robustness. These modules aim to handle and mitigate challenges associated with sparse and noisy graph structures.

## VII. CONCLUSION

In this study, we present DARKFARSEER, designed to mitigate the sparsity and noise present in real-world constructed graphs for ISK. We introduce a modeling paradigm specifically for virtual nodes and conduct an in-depth investigation into graph structure construction. We propose NHSE, which can be integrated with different GNNs to achieve significant performance improvements. We introduce VCCL, which alleviates potential graph sparsity by constructing BCCs and contrasting virtual nodes. We also present SGDS, which addresses potential graph density by using the feature similarity between virtual nodes and their neighbors. Extensive experiments demonstrate the superior performance of DARKFARSEER.

## REFERENCES

- [1] H. Zhou, S. Zhang, J. Peng, S. Zhang, J. Li, H. Xiong, and W. Zhang, “Informer: Beyond efficient transformer for long sequence time-series forecasting,” in *Proceedings of the AAAI conference on artificial intelligence*, vol. 35, no. 12, 2021, pp. 11 106–11 115.

- [2] M. Liu, A. Zeng, M. Chen, Z. Xu, Q. Lai, L. Ma, and Q. Xu, "Scinet: Time series modeling and forecasting with sample convolution and interaction," *Advances in Neural Information Processing Systems*, vol. 35, pp. 5816–5828, 2022.
- [3] S. V. Belavadi, S. Rajagopal, R. Ranjani, and R. Mohan, "Air quality forecasting using lstm rnn and wireless sensor networks," *Procedia Computer Science*, vol. 170, pp. 241–248, 2020.
- [4] Y. Wu, D. Zhuang, A. Labbe, and L. Sun, "Inductive graph neural networks for spatiotemporal kriging," in *Proceedings of the AAAI Conference on Artificial Intelligence*, vol. 35, no. 5, 2021, pp. 4478–4485.
- [5] Q. Xu, C. Long, Z. Li, S. Ruan, R. Zhao, and Z. Li, "Kits: Inductive spatio-temporal kriging with increment training strategy," *arXiv preprint arXiv:2311.02565*, 2023.
- [6] C. Zheng, X. Fan, C. Wang, J. Qi, C. Chen, and L. Chen, "Increase: Inductive graph representation learning for spatio-temporal kriging," in *Proceedings of the ACM Web Conference 2023*, 2023, pp. 673–683.
- [7] Z. Li, Y. Nie, Z. Li, L. Bai, Y. Lv, and R. Zhao, "Non-neighbors also matter to kriging: A new contrastive-prototypical learning," in *International Conference on Artificial Intelligence and Statistics*. PMLR, 2024, pp. 46–54.
- [8] G. Appleby, L. Liu, and L.-P. Liu, "Kriging convolutional networks," in *Proceedings of the AAAI Conference on Artificial Intelligence*, vol. 34, no. 04, 2020, pp. 3187–3194.
- [9] J. Hu, Y. Liang, Z. Fan, L. Liu, Y. Yin, and R. Zimmermann, "Decoupling long-and short-term patterns in spatiotemporal inference," *IEEE Transactions on Neural Networks and Learning Systems*, 2023.
- [10] T. Wei, Y. Lin, S. Guo, Y. Lin, Y. Zhao, X. Jin, Z. Wu, and H. Wan, "Inductive and adaptive graph convolution networks equipped with constraint task for spatial-temporal traffic data kriging," *Knowledge-Based Systems*, vol. 284, p. 111325, 2024.
- [11] J. Liu, H. Huang, J. Cao, and R. He, "Zepo: Zero-shot portrait stylization with faster sampling," in *Proceedings of the 32nd ACM International Conference on Multimedia*, 2024, pp. 3509–3518.
- [12] Y. Jing, Y. Yang, Z. Feng, J. Ye, Y. Yu, and M. Song, "Neural style transfer: A review," *IEEE transactions on visualization and computer graphics*, vol. 26, no. 11, pp. 3365–3385, 2019.
- [13] Y. Ma, Z. Song, X. Hu, J. Li, Y. Zhang, and I. King, "Graph component contrastive learning for concept relatedness estimation," in *Proceedings of the AAAI Conference on Artificial Intelligence*, vol. 37, no. 11, 2023, pp. 13 362–13 370.
- [14] J. Li, P. Zhou, C. Xiong, and S. Hoi, "Prototypical contrastive learning of unsupervised representations," in *International Conference on Learning Representations*, 2021. [Online]. Available: <https://openreview.net/forum?id=KmykpuSrjcg>
- [15] M. Jin, H. Y. Koh, Q. Wen, D. Zambon, C. Alippi, G. I. Webb, I. King, and S. Pan, "A survey on graph neural networks for time series: Forecasting, classification, imputation, and anomaly detection," *IEEE Transactions on Pattern Analysis and Machine Intelligence*, 2024.
- [16] Z. Wu, S. Pan, G. Long, J. Jiang, and C. Zhang, "Graph wavenet for deep spatial-temporal graph modeling," in *Proceedings of the 28th International Joint Conference on Artificial Intelligence*, 2019, pp. 1907–1913.
- [17] C. Song, Y. Lin, S. Guo, and H. Wan, "Spatial-temporal synchronous graph convolutional networks: A new framework for spatial-temporal network data forecasting," in *Proceedings of the AAAI conference on artificial intelligence*, vol. 34, no. 01, 2020, pp. 914–921.
- [18] C. Shang, J. Chen, and J. Bi, "Discrete graph structure learning for forecasting multiple time series," in *International Conference on Learning Representations*.
- [19] Y. Liu, Q. Liu, J.-W. Zhang, H. Feng, Z. Wang, Z. Zhou, and W. Chen, "Multivariate time-series forecasting with temporal polynomial graph neural networks," *Advances in neural information processing systems*, vol. 35, pp. 19414–19426, 2022.
- [20] Y. Cui, K. Zheng, D. Cui, J. Xie, L. Deng, F. Huang, and X. Zhou, "Metro: a generic graph neural network framework for multivariate time series forecasting," *Proceedings of the VLDB Endowment*, vol. 15, no. 2, pp. 224–236, 2021.
- [21] A. Cini, D. Mandic, and C. Alippi, "Graph-based time series clustering for end-to-end hierarchical forecasting," in *Forty-first International Conference on Machine Learning*.
- [22] Z. Li, L. Xia, Y. Xu, and C. Huang, "Gpt-st: generative pre-training of spatio-temporal graph neural networks," *Advances in Neural Information Processing Systems*, vol. 36, 2024.
- [23] A. Zeng, M. Chen, L. Zhang, and Q. Xu, "Are transformers effective for time series forecasting?" in *Proceedings of the AAAI conference on artificial intelligence*, vol. 37, no. 9, 2023, pp. 11 121–11 128.
- [24] Y. Nie, N. H. Nguyen, P. Sinthong, and J. Kalagnanam, "A time series is worth 64 words: Long-term forecasting with transformers," in *The Eleventh International Conference on Learning Representations*, 2023. [Online]. Available: <https://openreview.net/forum?id=Jbdc0vTOcol>
- [25] L. Han, H.-J. Ye, and D.-C. Zhan, "The capacity and robustness trade-off: Revisiting the channel independent strategy for multivariate time series forecasting," *IEEE Transactions on Knowledge and Data Engineering*, 2024.
- [26] J. Dong, H. Wu, H. Zhang, L. Zhang, J. Wang, and M. Long, "Simmtm: A simple pre-training framework for masked time-series modeling," *Advances in Neural Information Processing Systems*, vol. 36, 2024.
- [27] A. Cini, I. Marisca, and C. Alippi, "Filling the g\_ap\_s: Multivariate time series imputation by graph neural networks," in *International Conference on Learning Representations*, 2022. [Online]. Available: <https://openreview.net/forum?id=kOu3-S3wJ7>
- [28] Q. Ma, Z. Zhang, X. Zhao, H. Li, H. Zhao, Y. Wang, Z. Liu, and W. Wang, "Rethinking sensors modeling: Hierarchical information enhanced traffic forecasting," in *Proceedings of the 32nd ACM International Conference on Information and Knowledge Management*, 2023, pp. 1756–1765.
- [29] T. Zhang, R. Xu, C. Wang, Z. Duan, C. Chen, M. Qiu, D. Cheng, X. He, and W. Qian, "Learning knowledge-enhanced contextual language representations for domain natural language understanding," in *Proceedings of the 2023 Conference on Empirical Methods in Natural Language Processing*, 2023, pp. 15 663–15 676.
- [30] K. He, H. Fan, Y. Wu, S. Xie, and R. Girshick, "Momentum contrast for unsupervised visual representation learning," in *Proceedings of the IEEE/CVF conference on computer vision and pattern recognition*, 2020, pp. 9729–9738.
- [31] Y. Yan, R. Li, S. Wang, F. Zhang, W. Wu, and W. Xu, "Consert: A contrastive framework for self-supervised sentence representation transfer," in *Proceedings of the 59th Annual Meeting of the Association for Computational Linguistics and the 11th International Joint Conference on Natural Language Processing (Volume 1: Long Papers)*, 2021, pp. 5065–5075.
- [32] Z. Yue, Y. Wang, J. Duan, T. Yang, C. Huang, Y. Tong, and B. Xu, "Ts2vec: Towards universal representation of time series," in *Proceedings of the AAAI Conference on Artificial Intelligence*, vol. 36, no. 8, 2022, pp. 8980–8987.
- [33] J.-Y. Franceschi, A. Dieuleveut, and M. Jaggi, "Unsupervised scalable representation learning for multivariate time series," *Advances in neural information processing systems*, vol. 32, 2019.
- [34] Q. Meng, H. Qian, Y. Liu, L. Cui, Y. Xu, and Z. Shen, "Mhcl: masked hierarchical cluster-wise contrastive learning for multivariate time series," in *Proceedings of the AAAI Conference on Artificial Intelligence*, vol. 37, no. 8, 2023, pp. 9153–9161.
- [35] M. T. Nonnenmacher, L. Oldenburg, I. Steinwart, and D. Reeb, "Utilizing expert features for contrastive learning of time-series representations," in *International Conference on Machine Learning*. PMLR, 2022, pp. 16 969–16 989.
- [36] R. Tarjan, "Depth-first search and linear graph algorithms," *SIAM journal on computing*, vol. 1, no. 2, pp. 146–160, 1972.
- [37] J. Ji, J. Wang, C. Huang, J. Wu, B. Xu, Z. Wu, J. Zhang, and Y. Zheng, "Spatio-temporal self-supervised learning for traffic flow prediction," in *Proceedings of the AAAI conference on artificial intelligence*, vol. 37, no. 4, 2023, pp. 4356–4364.
- [38] A. v. d. Oord, Y. Li, and O. Vinyals, "Representation learning with contrastive predictive coding," *arXiv preprint arXiv:1807.03748*, 2018.
- [39] J. Fox and S. Rajamanickam, "How robust are graph neural networks to structural noise?" *arXiv preprint arXiv:1912.10206*, 2019.
- [40] J. Gilmer, S. S. Schoenholz, P. F. Riley, O. Vinyals, and G. E. Dahl, "Neural message passing for quantum chemistry," in *International conference on machine learning*. PMLR, 2017, pp. 1263–1272.
- [41] D. Luo, W. Cheng, W. Yu, B. Zong, J. Ni, H. Chen, and X. Zhang, "Learning to drop: Robust graph neural network via topological denoising," in *Proceedings of the 14th ACM international conference on web search and data mining*, 2021, pp. 779–787.
- [42] E. Dai, W. Jin, H. Liu, and S. Wang, "Towards robust graph neural networks for noisy graphs with sparse labels," in *Proceedings of the Fifteenth ACM International Conference on Web Search and Data Mining*, 2022, pp. 181–191.
- [43] E. Dai, T. Zhao, H. Zhu, J. Xu, Z. Guo, H. Liu, J. Tang, and S. Wang, "A comprehensive survey on trustworthy graph neural networks: Privacy, robustness, fairness, and explainability," *Machine Intelligence Research*, pp. 1–51, 2024.
- [44] W. Ju, S. Yi, Y. Wang, Z. Xiao, Z. Mao, H. Li, Y. Gu, Y. Qin, N. Yin, S. Wang et al., "A survey of graph neural networks in real

world: Imbalance, noise, privacy and ood challenges,” *arXiv preprint arXiv:2403.04468*, 2024.

- [45] Y. Wu, D. Zhuang, M. Lei, A. Labbe, and L. Sun, “Spatial aggregation and temporal convolution networks for real-time kriging,” *arXiv preprint arXiv:2109.12144*, 2021.
- [46] W. Cao, D. Wang, J. Li, H. Zhou, L. Li, and Y. Li, “Brits: Bidirectional recurrent imputation for time series,” *Advances in neural information processing systems*, vol. 31, 2018.
- [47] T. Zhou, H. Shan, A. Banerjee, and G. Sapiro, “Kernelized probabilistic matrix factorization: Exploiting graphs and side information,” in *Proceedings of the 2012 SIAM international Conference on Data mining*. SIAM, 2012, pp. 403–414.
- [48] M. T. Bahadori, Q. R. Yu, and Y. Liu, “Fast multivariate spatio-temporal analysis via low rank tensor learning,” *Advances in neural information processing systems*, vol. 27, 2014.
- [49] K. Takeuchi, H. Kashima, and N. Ueda, “Autoregressive tensor factorization for spatio-temporal predictions,” in *2017 IEEE international conference on data mining (ICDM)*. IEEE, 2017, pp. 1105–1110.
- [50] D. Xu, C. Wei, P. Peng, Q. Xuan, and H. Guo, “Ge-gan: A novel deep learning framework for road traffic state estimation,” *Transportation Research Part C: Emerging Technologies*, vol. 117, p. 102635, 2020.
- [51] Y. Zhang, A. Li, J. Li, D. Han, T. Li, R. Zhang, and Y. Zhang, “Speckriging: Gnn-based secure cooperative spectrum sensing,” *IEEE Transactions on Wireless Communications*, vol. 21, no. 11, pp. 9936–9946, 2022.
- [52] Y. Li, R. Yu, C. Shahabi, and Y. Liu, “Diffusion convolutional recurrent neural network: Data-driven traffic forecasting,” in *International Conference on Learning Representations*, 2018. [Online]. Available: <https://openreview.net/forum?id=SJiHXGWAZ>
- [53] W. Hamilton, Z. Ying, and J. Leskovec, “Inductive representation learning on large graphs,” *Advances in neural information processing systems*, vol. 30, 2017.
- [54] J. Ye, Z. Liu, B. Du, L. Sun, W. Li, Y. Fu, and H. Xiong, “Learning the evolutionary and multi-scale graph structure for multivariate time series forecasting,” in *Proceedings of the 28th ACM SIGKDD conference on knowledge discovery and data mining*, 2022, pp. 2296–2306.
- [55] K. Zhao, C. Guo, Y. Cheng, P. Han, M. Zhang, and B. Yang, “Multiple time series forecasting with dynamic graph modeling,” *Proceedings of the VLDB Endowment*, vol. 17, no. 4, pp. 753–765, 2023.
- [56] Z. L. Li, G. W. Zhang, J. Yu, and L. Y. Xu, “Dynamic graph structure learning for multivariate time series forecasting,” *Pattern Recognition*, vol. 138, p. 109423, 2023.
- [57] H. Liu, D. Yang, X. Liu, X. Chen, Z. Liang, H. Wang, Y. Cui, and J. Gu, “Todynnet: temporal dynamic graph neural network for multivariate time series classification,” *Information Sciences*, p. 120914, 2024.
- [58] J. Wu, Q. Qi, J. Wang, H. Sun, Z. Wu, Z. Zhuang, and J. Liao, “Not only pairwise relationships: Fine-grained relational modeling for multivariate time series forecasting,” in *IJCAI*, 2023, pp. 4416–4423.
- [59] N. Yin, L. Shen, H. Xiong, B. Gu, C. Chen, X.-S. Hua, S. Liu, and X. Luo, “Messages are never propagated alone: Collaborative hypergraph neural network for time-series forecasting,” *IEEE Transactions on Pattern Analysis and Machine Intelligence*, 2023.
- [60] Z. Shang and L. Chen, “Mshyper: Multi-scale hypergraph transformer for long-range time series forecasting,” *arXiv preprint arXiv:2401.09261*, 2024.
- [61] S. Qin, L. Chen, Y. Luo, and G. Tao, “Multi-view graph contrastive learning for multivariate time series anomaly detection in iot,” *IEEE Internet of Things Journal*, 2023.
- [62] Y. Wang, Y. Xu, J. Yang, M. Wu, X. Li, L. Xie, and Z. Chen, “Graph contextual contrasting for multivariate time series classification,” *arXiv preprint arXiv:2309.05202*, 2023.



**Zhuoxuan Liang** received his B.S. degree in Internet of Things Engineering from Henan University of Engineering, Zhengzhou, China, in 2022. He is currently pursuing his M.S. degree in the College of Computer Science and Technology at Harbin Engineering University, Harbin, China. His research interests focus on spatio-temporal data mining and image processing.



**Wei Li** received the B.E. and M.Sc. degrees in computer science and technology from Wuhan University and Harbin Institute of Technology, in 2012 and 2015, respectively. He got a Ph.D. degree from the School of Computer Science and Engineering, the University of New South Wales, in 2019. He is currently an Associate Professor in the College of Computer Science and Technology, Harbin Engineering University, China. His research interests include the fields of (big) graph analytics and spatio-temporal data mining.



**Dalin Zhang** received his B.Sc. and M.Sc. degrees from Jilin University and University of Chinese Academy of Sciences, in 2012 and 2015, respectively. Afterwards, he worked as a digital design engineer at Spreadtrum Inc. and then got his Ph.D. degree from the School of Computer Science and Engineering, the University of New South Wales, in 2020. His research interests include spatio-temporal data mining, brain-computer interface, and the Internet of Things.



**Yidan Chen** received the B.S. degree in information and computing science in June 2021. He is pursuing an M.S. degree in the College of Computer Science and Technology at Harbin Engineering University. His research interests include Database, Community Detection and Densest Subgraph Discovery.



**Zhihong Wang** received the M.E. degree in Computer Science and Technology from Fujian Agriculture and Forestry University, fuzhou, China, in 2022. He is currently pursuing the Ph.D. degree with the School of Computer Science and Technology, Harbin Engineering University, Harbin, China. His current research interests include anomaly detection, data mining, and recommender systems.



**Xiangping Zheng** received the Ph.D. degree in Computer Application Technology from the Information School, Renmin University of China. He is currently an Assistant Professor and a master's Supervisor with Harbin Engineering University. His research interests include graph data mining and information retrieval. He is a member of ACM and a member of CCF.



**Moustafa Youssef** is a full Professor at the American University in Cairo, Egypt. He is the founder & director of the Wireless Research Center of Excellence, Egypt. His research interests include mobile wireless networks, mobile computing, location determination technologies, pervasive computing, and quantum computing. He is an Associate Editor for IEEE TMC and ACM TSAS. He is also an IEEE and ACM Fellow.